Draft version March 5, 2024
Typeset using LaTeX twocolumn style in AASTeX631

Radiation Process in Relativistic MHD Waves: the Case of Circularly Polarized Alfvén Wave

Ryota Goto[1] and Katsuaki Asano[1]

[1] Institute for Cosmic Ray Research, The University of Tokyo, 5-1-5 Kashiwanoha, Kashiwa, Chiba 277-8582, Japan

ABSTRACT

Turbulence in highly magnetized plasma can be relativistic and induce an electric field comparable to the background magnetic field. Such a strong electric field can affect the emission process of non-thermal electrons. As the first step toward elucidating the emission process in relativistic turbulence, we study the radiation process of electrons in relativistic circularly polarized Alfvén waves. While the induced electric field boosts the average energy of low-energy electrons with a Larmor radius smaller than the wavelength, the emissivity for such electrons is suppressed because of the elongated gyro-motion trajectory. The trajectory of high-energy electrons is shaken by the small-scale electric field, which enhances the emissivity. Since the effective Lorentz factor of $E \times B$ drift is $\simeq \sqrt{2}$ in the circularly polarized Alfvén waves, the deviation from the standard synchrotron emission is not so prominent. However, a power-law energy injection in the waves can produce a concave photon spectrum, which is similar to the GeV extra component seen in GRB spectra. If the turbulence electric field is responsible for the GeV extra component in GRBs, the estimates of the typical electron energy and magnetic field should be largely altered.

1. INTRODUCTION

The most promising launching mechanism of relativistic jets is the Blandford–Znajek mechanism (Blandford & Znajek 1977), where the rotation energy of a black hole is extracted via a magnetic field in the ergosphere. In this case, the jet energy is dominated by the magnetic field(McKinney et al. 2012, 2014). Relativistic winds from pulsars or magnetars are also dominated by magnetic fields (Goldreich & Julian 1969).

Turbulence may be driven by kink instability or magnetic reconnection in the magnetically dominated (high-σ) outflows(Begelman 1998; Mizuno et al. 2009, 2011; Porth et al. 2014; Porth & Komissarov 2015; Tchekhovskoy & Bromberg 2016; Bromberg & Tchekhovskoy 2016; Singh et al. 2016). The turbulence induced in highly magnetized plasma can be responsible for the dissipation of the magnetic field via turbulence reconnection and particle acceleration (Guo et al. 2015; Nalewajko et al. 2015; Takamoto et al. 2015; Zhdankin et al. 2017; Werner & Uzdensky 2017; Petropoulou & Sironi 2018; Guo et al. 2019; Hakobyan et al. 2019; Comisso & Sironi 2019; Wong et al. 2020; Comisso et al. 2020; Guo et al. 2021; Hakobyan et al. 2021). Large amplitude turbulent components of magnetic fields and turbulent motions have been suggested from the observed image and polarization in Crab nebula (Shibata et al. 2003; Lyutikov 2010; Bucciantini et al. 2017; Mizuno et al. 2023). In gamma-ray bursts (GRBs) and blazars, the time variability of the flux and polarization may be due to turbulence (Lazar et al. 2009; Narayan & Kumar 2009; Zhang & Zhang 2014; Marscher 2014). Thus, the photon emission from relativistic flows in GRBs, blazars and pulsar wind nebulae (PWNe) can originate from particles in turbulence in high-σ plasma.

In high-σ plasma, the Alfvén velocity is almost the speed of light. The turbulence velocity can be relativistic. In such turbulence, the induced electric field is comparable to the magnetic field. The electric field affects the trajectory of non-thermal charged particles so that the emission property can be different from the standard synchrotron emission. In most cases, the magnetic fields in the emission region have been estimated by spectral modeling with the standard synchrotron, inverse Compton, and π^0-decay processes. If the synchrotron emission is largely modified by the turbulence electric field, the estimate of the magnetic field may be misinterpreted.

In this paper, as the first step toward unveiling the emission property in high-σ turbulence, we investigate the radiation process in relativistic circularly polarized Alfvén waves, which is analytically described.

The structure of this paper is as follows. In Section 2, we review the radiation process in the uniform electric field case. In Section 3, we discuss the emission properties in a relativistic circularly polarized Alfvén wave. In Section 4, our numerical method to calculate radiation from electron trajectories is shown. In Section 5, we show the numerical results of the radiation for mono-energetic and power-law injections of electrons. In Section 7, we summarize our results and discuss their implication for spectral modeling.

2. UNIFORM ELECTRIC FIELD

In the ideal magnetohydrodynamics (MHD), relativistic turbulece with a turbulent velocity $\delta V \sim c$ induces the motional electric field with a strength $|\boldsymbol{E}| = |\frac{\boldsymbol{\delta V}}{c} \times \boldsymbol{B}|$, which can be comparable to the magnetic field strength $|\boldsymbol{B}|$. The radiation process of charged particles in such relativistic turbulence can be different from conventional synchrotron radiation. In this section, to clarify the effect of an electric field, we first review the radiation process of electrons in the uniform field case.

When a uniform electric field $\boldsymbol{E}$ is perpendicular to a uniform magnetic field $\boldsymbol{B}$, an observer moving with the drift velocity $\boldsymbol{v}_{E\times B} = c\frac{\boldsymbol{E}\times\boldsymbol{B}}{B^2}$ observes zero electric field as long as $E < B$. The corresponding $E \times B$ drift Lorentz factor is

$$\Gamma_{E\times B} = \frac{1}{\sqrt{1-\frac{E^2}{B^2}}}. \tag{1}$$

In this frame (drifting frame), the motion of electrons is spiral around the magnetic field $B' = B/\Gamma_{E\times B}$, and the emission from electrons is the usual synchrotron radiation in the manetic field B'. (Hereafter, the prime $'$ denotes quantities in the drifting frame.) Considering electrons isotropically injected with a Lorentz factor $\gamma_{\rm i}$ in the original frame, the synchrotron power, namely photon energy emitted per unit time is given by(Rybicki & Lightman 1979; Jackson & Fox 1999)

$$P'_{\rm syn} \simeq 2\gamma'^2 c\sigma_{\rm T}\frac{B'^2}{8\pi}, \tag{2}$$

where $\gamma' \sim \Gamma_{E\times B}\gamma_{\rm i}$ is the typical Lorentz factor of the electrons in the drifting frame, and $\sigma_{\rm T}$ is the Thomson scattering cross section.

In the original frame, the time-averaged Lorentz factor of the electrons is

$$\gamma_{\rm ave} \simeq \Gamma_{E\times B}\gamma' \simeq \Gamma_{E\times B}^2\gamma_{\rm i}. \tag{3}$$

The average energy is boosted from the injection value by the electric field. The drift motion of a charged particle in fields of $E \simeq B$ is elongated in the direction of the drift velocity. This asymmetric motion stretches the time interval for $\gamma > \gamma_{\rm ave}$. As explained in Appendix, this effect slightly increases $\gamma_{\rm ave}$ compared to the above estimate. The radiation power is Lorentz invariant(Rybicki & Lightman 1979; Jackson & Fox 1999). Using γ, the radiation power is written as

$$P_{E\times B} = P'_{\rm syn} \simeq \frac{1}{\Gamma_{E\times B}^4} 2\gamma_{\rm ave}^2 c\sigma_{\rm T}\frac{B^2}{8\pi}. \tag{4}$$

The radiation power is suppressed by the factor $1/\Gamma_{E\times B}^4$ compared to the usual synchrotron formula without an electric field. In Appendix, we show more details of analytically calculations of the radiation power.

3. RADIATION IN ALFVÉN WAVE

In astrophysical MHD turbulence, there may be a frame where the turbulence is globally isotropic, but locally the fluid velocity and the electromagnetic field are anisotropic. For simplicity, we assume that electrons are isotropically injected in this frame. The turbulence may be injected at a large scale, and cascade into smaller scales, where the wave amplitude of the turbulence is so small ($\delta V \ll c$) that the effect of the electric field is almost negligible. The induced electric field is significant only at the injection scale. To investigate the effect of the turbulence electric field on the radiation, we consider a wave propagating to a certain direction with a finite wave length λ. While various modes of MHD waves as turbulence are possible, the analytical description is possible for circularly polarized Alfvén waves even with non-linear amplitude ($\delta V \sim c$). As a first step, here we focus on this simplest case.

3.1. *Circularly polarized Alfvén wave*

Relativistic perturbation ($\delta V \sim c$) implies non-linear amplitudes of the perturbed fields. Even in linearly polarized Alfvén waves, the induced magnetic pressure leads to compression of fluid. The compressed part of the waves propagates faster and the nonlinear waves steepen (Shikin 1969), so that the analytical description of the non-linear Alfvén waves is difficult. On the other hand, the circularly polarized Alfvén wave can be treated with a constant total pressure in any phase of the wave.

The analytical description of the perturbed electromagnetic fields for a relativistic circularly polarized Alfvén wave propagating along the background magnetic field (z-axis) is given by (Kennel & Pellat 1976)

$$B_z = B_0, \tag{5}$$

$$\delta E_z = 0, \tag{6}$$

$$\delta B_x = -B_0\frac{V}{V_{\rm A}}\cos(kz-\omega_{\rm A}t), \tag{7}$$

$$\delta B_y = -B_0\frac{V}{V_{\rm A}}\sin(kz-\omega_{\rm A}t), \tag{8}$$

$$\delta E_x = -B_0\frac{V}{c}\sin(kz-\omega_{\rm A}t), \tag{9}$$

$$\delta E_y = B_0\frac{V}{c}\cos(kz-\omega_{\rm A}t), \tag{10}$$

where B_0 is the strength of the background magnetic field, V is the fluid velocity in the Alfvén wave, and $k = 2\pi/\lambda$ is the wavenumber. Given the gas energy density ε and the gas pressure p, the phase speed of the Alfvén wave is written as $V_{\rm A} = \omega_{\rm A}/k = cB_0/\sqrt{B_0^2 + 4\pi(\varepsilon+p)\Gamma^2}$, where $\Gamma = 1/\sqrt{1-(V/c)^2}$. Introducing the magnetization parameter $\sigma = B_0^2/(4\pi(\varepsilon+p)\Gamma^2)$, the phase speed is rewritten as $V_{\rm A} = c\sqrt{\sigma/(\sigma+1)}$. As shown in equations (5)-(10), for $V \sim V_{\rm A} \sim c$, the induced electric field is comparable to the background magnetic field.

3.2. *Long wavelength limit*

In this section, we consider the case in which the Larmor radius of electrons is much smaller than the wavelength,

$$r_{\rm L0} \equiv \frac{\gamma_{\rm i} m_e c^2}{eB_0} \ll \lambda. \tag{11}$$

In this case, the electric and magnetic fields can be approximated as almost uniform ones. The radiation power of electrons is suppressed as $P_{\rm ave} \simeq \frac{1}{\Gamma_{E\times B}^4} 2\gamma_{\rm ave}^2 c\sigma_T \frac{B^2}{8\pi}$ as discussed in section 2, where

$$B^2 = B_0^2 + \delta B^2. \tag{12}$$

In the circularly polarized Alfvén wave with $B_0 \simeq \delta B \simeq \delta E$, the $E \times B$ drift velocity is

$$\beta_{E\times B} = \frac{E}{B} = \frac{\delta E}{\sqrt{B_0^2 + \delta B^2}} \simeq \frac{1}{\sqrt{2}}, \tag{13}$$

which implies $\Gamma_{E\times B} \simeq \sqrt{2}$. Finally, we obtain

$$P_{\rm ave} \simeq \gamma_{\rm ave}^2 c\sigma_T \frac{B^2}{16\pi}. \tag{14}$$

From the Lorentz transformation of the synchrotron frequency in the $E \times B$ rest frame, the typical frequency is

$$\begin{aligned}\nu_{\rm typ} &\simeq D\frac{3}{4\pi}\gamma'^2\frac{eB'}{m_e c}\sin\alpha' \\ &\simeq \frac{1}{\Gamma_{E\times B}^2}\frac{3}{4\pi}\gamma_{\rm ave}^2\frac{eB}{m_e c} \simeq \frac{\frac{4}{\pi}}{\Gamma_{E\times B}^2}\nu_0,\end{aligned} \tag{15}$$

where $D \simeq \Gamma_{E\times B}$ is the Doppler factor, $B' = B/\Gamma_{E\times B}$, $\gamma' \simeq \gamma_{\rm ave}/\Gamma_{E\times B}$ and

$$\nu_0 \equiv \frac{3}{16}\gamma_{\rm ave}^2\frac{eB}{m_e c}, \tag{16}$$

is the typical frequency of isotropic synchrotron radiation. The typical frequency decreases by the factor $\frac{4}{\pi}/\Gamma_{E\times B}^2 \simeq 2/\pi$ compared to the usual synchrotron formula.

3.3. *Short wavelength limit*

In the case with $r_{\rm L0} \gg \lambda$, frequent changes of the field directions should be taken into account. The radiation power of an electron (charge $-e$) is given by the Liénard formula(Schwinger 1949),

$$P = \frac{2e^2}{3c^3}\gamma^4(a_\perp^2 + \gamma^2 a_\parallel^2), \tag{17}$$

where $a_\perp$ and $a_\parallel$ are perpendicular and parallel components of acceleration, respectively.

From the equation of motion

$$\frac{d\gamma m_e \boldsymbol{v}}{dt} = -e\boldsymbol{E} - e\frac{\boldsymbol{v}}{c}\times\boldsymbol{B}, \tag{18}$$

and the energy conservation

$$\frac{d\gamma m_e c^2}{dt} = -e\boldsymbol{E}\cdot\boldsymbol{v}, \tag{19}$$

we obtain acceleration of an electron as

$$\boldsymbol{a} = -\frac{e}{\gamma m_e}\left(\boldsymbol{E} - \frac{\boldsymbol{v}}{c}\left(\frac{\boldsymbol{v}}{c}\cdot\boldsymbol{E}\right) + \frac{\boldsymbol{v}}{c}\times\boldsymbol{B}\right). \tag{20}$$

Then, we obtain the parallel component as

$$a_\parallel = \boldsymbol{a}\cdot\frac{\boldsymbol{v}}{v} = -\frac{e}{\gamma^3 m_e}\frac{\boldsymbol{v}}{v}\cdot\boldsymbol{E}, \tag{21}$$

and the perpendicular component as

$$\begin{aligned}\boldsymbol{a}_\perp &= \boldsymbol{a} - a_\parallel\frac{\boldsymbol{v}}{v} \\ &= -\frac{e}{\gamma m_e}\left(\boldsymbol{E} - \frac{\boldsymbol{v}}{v}\left(\frac{\boldsymbol{v}}{v}\cdot\boldsymbol{E}\right) + \frac{\boldsymbol{v}}{c}\times\boldsymbol{B}\right).\end{aligned} \tag{22}$$

For $\gamma \gg 1$, equations (21) and (22) imply

$$a_\perp^2 + \gamma^2 a_\parallel^2 \simeq a_\perp^2, \tag{23}$$

which leads to(Schwinger 1949)

$$P \simeq \frac{\gamma^2 c\sigma_T}{4\pi}\left(\boldsymbol{E} - \frac{\boldsymbol{v}}{v}\left(\frac{\boldsymbol{v}}{v}\cdot\boldsymbol{E}\right) + \frac{\boldsymbol{v}}{c}\times\boldsymbol{B}\right)^2. \tag{24}$$

From equation (19) with $\delta B \simeq \delta E \simeq B_0$, the fractional change of the Lorentz factor during the wave crossing time $\Delta t = \lambda/v$ is

$$\frac{\Delta\gamma}{\gamma} \sim \frac{\Delta t}{\gamma}\frac{d\gamma}{dt} \sim \frac{\lambda e B_0}{\gamma m_e c^2} \sim \frac{\lambda}{r_{\rm L0}} \ll 1. \tag{25}$$

Similarly, equation (18) gives the angle change as

$$\Delta\theta \simeq \frac{\Delta t}{\gamma m_e v}\frac{d\gamma m_e v_\perp}{dt} \simeq \frac{\lambda e B_0}{\gamma m_e c^2} \simeq \frac{\lambda}{r_{\rm L0}} \ll 1. \tag{26}$$

Therefore, the electron trajectory is a spiral motion around the background magnetic field with a small oscillation. The velocity components of an electron injected with a pitch angle $\theta_{\rm i}$ and an azimuthal angle $\phi_{\rm i}$ are approximately expressed as

$$\gamma \simeq \gamma_{\rm i} \simeq \gamma_{\rm ave}, \tag{27}$$

$$v_x \simeq v \sin\theta_{\rm i} \cos(\omega_B t + \phi_{\rm i}), \tag{28}$$

$$v_y \simeq v \sin\theta_{\rm i} \sin(\omega_B t + \phi_{\rm i}), \tag{29}$$

$$v_z \simeq v \cos\theta_{\rm i}, \tag{30}$$

where $\omega_B = \frac{eB_0}{\gamma m_e c}$ is the gyro frequency.

As the electron injection is isotropic in this frame, we average over the angles $\theta_{\rm i}$, $\phi_{\rm i}$, and a time interval T much longer than the wave crossing time λ/v. Equations (5)-(10), (24) and (27)-(30) lead to

$$P_{\rm ave} \equiv \frac{1}{4\pi}\int_0^{2\pi} d\phi_{\rm i} \int_0^{\pi} d\theta_{\rm i} \sin\theta_{\rm i} \frac{1}{T}\int_0^T dt P(\gamma_{\rm i},\theta_{\rm i},\phi_{\rm i},t)$$
$$\simeq \frac{4}{3}\gamma_{\rm ave}^2 c\sigma_T\left(\frac{B_0^2}{8\pi}+\frac{\delta B^2}{8\pi}+\frac{\delta E^2}{8\pi}\right) \simeq \gamma_{\rm ave}^2 c\sigma_T \frac{B^2}{4\pi}, \tag{31}$$

where $B^2 = B_0^2 + \delta B^2$ again. Differently from the case for $\lambda \gg r_{\rm L0}$ in section 3.2, the radiation power is rather enhanced by the perturbed electric field.

We estimate the typical emission frequency. As we consider MHD turbulence, the Larmor radius of non-relativistic electrons is assumed to be short enough as $\lambda \gg m_e c^2/eB$. In this case, equation (26) implies $\lambda \gg r_{\rm L,0}/\gamma$, and $\Delta\theta \gg 1/\gamma$. This means that the radiation cone with opening angle $1/\gamma$ sweeps a certain position before an electron oscillates with a deflection angle $\Delta\theta$(Medvedev 2000). With $a \simeq a_\perp$, the emission frequency can be estimated (Reville & Kirk 2010) as

$$\nu(\theta_{\rm i},\phi_{\rm i},t) \equiv \frac{3\gamma^3(\theta_{\rm i},\phi_{\rm i},t)a_\perp(\theta_{\rm i},\phi_{\rm i},t)}{4\pi c}. \tag{32}$$

Averaging with the weight of the radiation power over the angles $\theta_{\rm i}, \phi_{\rm i}$ and time, we can obtain the typical emitted frequency

$$\nu_{\rm typ} \equiv \frac{1}{P_{\rm ave}}\frac{1}{4\pi}\int_0^{2\pi} d\phi_{\rm i}\int_0^{\pi} d\theta_{\rm i}\sin\theta_{\rm i}$$
$$\times\frac{1}{T}\int_0^T dt\nu(\theta_{\rm i},\phi_{\rm i},t)P(\theta_{\rm i},\phi_{\rm i},t). \tag{33}$$

In the case without the turbulence, assuming $\delta E = \delta B = 0$ and using equations (5)-(10), (22), (24) and (27)-(30), we numerically obtain

$$\nu_{\rm typ} \simeq 1.46\nu_0. \tag{34}$$

In the circularly polarized Alfvén wave, a similar calculation assuming $\delta E \simeq \delta B \simeq B_0$ leads to

$$\nu_{\rm typ} \simeq 2.11\nu_0. \tag{35}$$

The increase of the peak frequency is because the perturbed electric field δE increases the perpendicular acceleration $a_\perp$ in equation (22).

4. NUMERICAL METHOD

As we have mentioned, we assume that a monochromatic wave propagates along the z-axis as expressed by equations (5)-(10). The wave locally dominates the turbulence, which is globally isotropic. In the wave rest frame (moving along the z-axis with the velocity $V_{\rm A}$), the electric field vanishes. Neglecting the radiative cooling, the electron energy in the wave rest frame is conserved. The electron energy in the original frame periodically oscillates following the change of momentum in the wave rest frame. Therefore, the time averaged Lorentz factor in the original frame does not evolve in this circularly polarized Alfvén wave.

We isotropically inject electrons in the original frame, and solve the equations of motion

$$\frac{d\boldsymbol{x}}{dt} = \boldsymbol{v}, \tag{36}$$

$$\frac{d\gamma m_e \boldsymbol{v}}{dt} = -e\boldsymbol{E}(\boldsymbol{x},t) - e\frac{\boldsymbol{v}}{c}\times\boldsymbol{B}(\boldsymbol{x},t), \tag{37}$$

using the Boris-C solver with second-order accuracy in Zenitani & Umeda (2018) with a time step $\Delta t = 0.02\min(\lambda/c, r_{\rm L0}/c)$. We isotropically inject 1600 electrons in total.

The average Lorentz factor for electrons injected with a Lorentz factor $\gamma_{\rm i} \gg 1$ is calculated with a time interval $T = 200\min(\lambda/c, r_{\rm L0}/c)$ as

$$\gamma_{\rm ave}(\gamma_{\rm i}) \equiv \frac{1}{4\pi}\int_0^{2\pi} d\phi_{\rm i}\int_0^{\pi} d\theta_{\rm i}\sin\theta_{\rm i}\frac{1}{T}\int_0^T dt\gamma. \tag{38}$$

The radiation power is numerically calculated using the Liénard formula

$$P(\gamma_{\rm i},\theta_{\rm i},\phi_{\rm i},t) = \frac{2e^2}{3c^3}\gamma^4(a_\perp^2+\gamma^2 a_\parallel^2), \tag{39}$$

which is also averaged as

$$P_{\rm ave}(\gamma_{\rm ave}(\gamma_{\rm i})) \equiv \frac{1}{4\pi}\int_0^{2\pi} d\phi_{\rm i}\int_0^{\pi} d\theta_{\rm i}\sin\theta_{\rm i}$$
$$\times\frac{1}{T}\int_0^T dt P(\gamma_{\rm i},\theta_{\rm i},\phi_{\rm i},t). \tag{40}$$

The radiation power spectrum of an electron is given by the Fourier transformation of the radiation electric field described by the Liénard Wiechart potential (Rybicki & Lightman 1979; Jackson & Fox 1999). For $\lambda \gg m_e c^2/eB$ and $E \leq B$, the radiation spectrum can be approximately calculated (Reville & Kirk 2010) by

$$P(\nu,\gamma_{\rm i},\theta_{\rm i},\phi_{\rm i}) = \frac{1}{T}\int_0^T dt\frac{\sqrt{3}e^2\gamma a_\perp}{c^2}F\left(\frac{4\pi c\nu}{3\gamma^3 a_\perp}\right), \tag{41}$$

where $F(x) \equiv x\int_x^\infty K_{\frac{5}{3}}(\xi)d\xi$, and $K_{\frac{5}{3}}(\xi)$ is the modified Bessel function of the order 5/3. We resolve frequency range by 20 meshes per logbin. For calculation of $F(x)$, we interpolate the analytical approximate formula in Fouka & Ouichaoui (2013) by the cubic spline in every time step Δt.

The radiation spectrum is averaged over the injection angles $\theta_{\rm i}$ and $\phi_{\rm i}$ as

$$P_{\nu,\rm ave}(\gamma_{\rm ave}(\gamma_{\rm i})) = \frac{1}{4\pi}\int_0^{2\pi} d\phi_{\rm i}\int_0^{\pi} d\theta_{\rm i}\sin\theta_{\rm i} \times P(\nu,\gamma_{\rm i},\theta_{\rm i},\phi_{\rm i}). \quad (42)$$

5. MONO-ENERGETIC INJECTION

In this section, we show numerical results for electrons isotropically injected with an initial Lorentz factor $\gamma_{\rm i}$ for a parameter range of $10^{-5} \le r_{\rm L0}/\lambda \le 10^3$. As we mentioned, the MHD approximation implies $\lambda \gg m_e c^2/eB$. So the jitter radiation mechanism ($\lambda < m_e c^2/eB$, Medvedev 2000) is not eligible in our case. Our results are shown normalized by the well-known formulae for a uniform magnetic field: the radiation power

$$P_0 \equiv \frac{4}{3}\gamma_{\rm ave}^2 c\sigma_T \frac{B^2}{8\pi}, \quad (43)$$

and the typical frequency ν_0 given by eq. (15).

The upper panel of Figure 1 shows the average Lorentz factor $\gamma_{\rm ave}$ as a function of $r_{\rm L0}/\lambda$. In low energy limit ($r_{\rm L0}/\lambda \ll 1$), the electron energy is boosted by a factor of $2\times 1.19 \simeq 2.4$ as explained in section 2 and Appendix, while $\gamma_{\rm ave}$ is almost the sama as $\gamma_{\rm i}$ in high energy limit ($r_{\rm L0}/\lambda \ll 1$) as explained in §3.3. As shown in the lower panel of Figure 1, the radiation power for $r_{\rm L0}/\lambda \ll 1$ is suppressed by a factor of $1/\Gamma_{E\times B}^4 \simeq 1/4$ as estimated in equation (A10). On the other hand, the power is 1.5-fold enhanced by the electric field for $r_{\rm L0}/\lambda \gg 1$ as discussed in §3.3.

In Figure 2, we show the radiation spectra $\nu P_{\nu,\rm ave}/P_0$. In the case of $r_{\rm L0}/\lambda = 10^3$ (green), the radiation power is enhanced compared to the case without the turbulence (black). The peak frequency is also increased compared to the synchrotron case as discussed in §3.3.

For $r_{\rm L0}/\lambda = 10^{-5}$ (blue), the radiation power is suppressed compared to the case without the turbulence by a factor of $1/\Gamma_{E\times B} \simeq 1/4$. The slight decrease in the typical frequency is consistent with the discussion in equation (15).

The spectrum for $r_{\rm L0}/\lambda = 10^{-5}$ is broader than the other cases. The broadening is due to the dispersions in the Doppler factor $D = \Gamma_{E\times B}(1+\beta_{E\times B}\cos\theta')$ and the Lorentz factor in the $E\times B$ rest frame $\gamma' = \Gamma_{E\times B}\gamma_{\rm i}(1-\beta_{E\times B}\beta_0\cos\theta)$, where θ' and θ are the angles

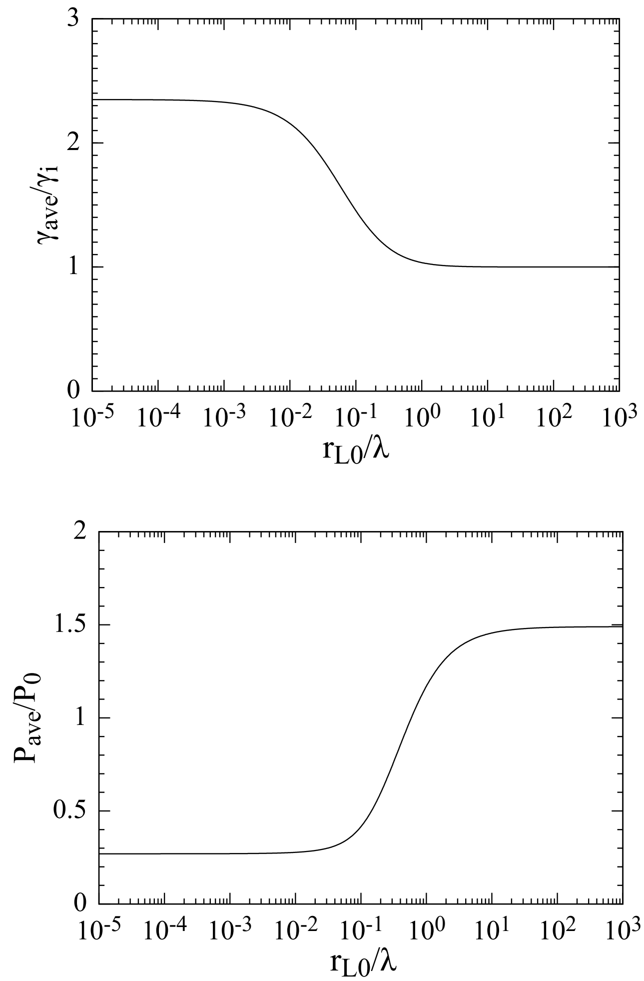

Figure 1. Upper: the average Lorentz factor $\gamma_{\rm ave}$ of electrons injected with Lorentz factor $\gamma_{\rm i}$. Lower: the average radiation power $P_{\rm ave}$ normalized by P_0.

of the propagation direction of photons and the electron motion direction at injection, respectively, with respect to the $E\times B$ drift velocity. The dispersions are significant for $r_{\rm L0} \ll \lambda$.

6. POWER-LAW INJECTION

In a strong magnetic field, the effect of radiative cooling appears in the high-energy electron energy distribution. Assuming a continuous electron injection with a power-law energy distribution and electron escape, a broken power-law energy distribution is frequently assumed as a steady state. In our case with relativistic turbulence, we need to consider not only cooling but also the energy boost by the electric field, shown in Figure 1.

6.1. *Method*

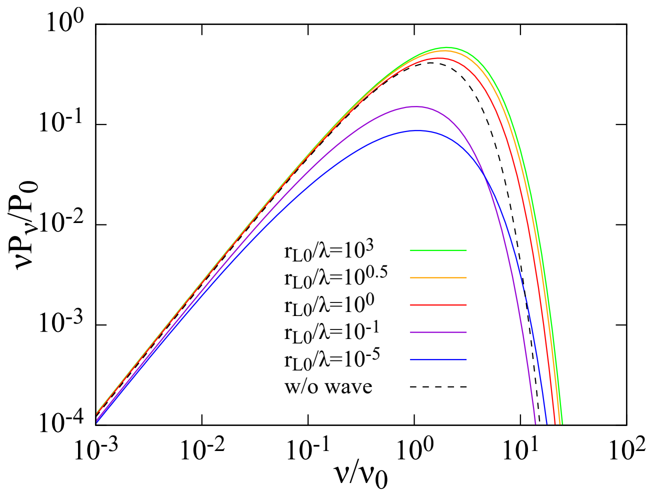

Figure 2. Radiation spectra for different $r_{\rm L0}/\lambda$. The synchrotron spectrum without the turbulence is shown with black line as a reference.

Depending on the cooling break in the electron energy distribution, the photon spectrum shows a variety. We numerically calculate the time evolution of electron energy distribution $N(\gamma, t)$ in a relativistic Alfvén wave by solving the equation of continuity in the energy space as

$$\frac{\partial N(\gamma_{\rm ave}, t)}{\partial t} + \frac{\partial}{\partial \gamma_{\rm ave}}(\dot{\gamma}_{\rm ave}(\gamma_{\rm ave})N(\gamma_{\rm ave}, t)) = \dot{N}_{\rm inj}(\gamma_{\rm ave}), \tag{44}$$

where $\dot{\gamma}_{\rm ave}(\gamma_{\rm ave})$ is radiative cooling rate of electrons in relativistic Alfvén wave and the injection term $\dot{N}_{\rm inj}(\gamma_{\rm ave})$ is assumed to be constant with time. By changing the calculation time t, the energy at the cooling break can be adjusted.

As shown in the upper panel of Figure 1, we take into account the boost of Lorentz factor of electrons after injection for the injected electron energy distribution. The initial electron energy distribution at injection is assumed as a power law distribution with an exponential cutoff as

$$\dot{N}_{\rm inj,0}(\gamma_{\rm i}) = C\gamma_{\rm i}^{-p}\exp\left(-\frac{\gamma_{\rm i}}{\gamma_{\rm cut}}\right) \quad \text{for} \quad \gamma_{\rm min} < \gamma_{\rm i} < \gamma_{\rm max}, \tag{45}$$

where $\gamma_{\rm i}$ is the initial Lorentz factor at injection and $C = 1/\int_{\gamma_{\rm min}}^{\gamma_{\rm max}} d\gamma_{\rm i}\dot{N}_{\rm inj,0}(\gamma_{\rm i})t$ is the normalization factor. In this paper, we adopt $p = 2$. Then, we calculate the electron distribution after the energy boost by the wave using $\gamma_{\rm ave}(\gamma_{\rm i})$ calculated with equation (38) as

$$\dot{N}_{\rm inj}(\gamma_{\rm ave}) = \frac{d\gamma_{\rm i}}{d\gamma_{\rm ave}}\dot{N}_{\rm inj,0}(\gamma_{\rm i}(\gamma_{\rm ave})). \tag{46}$$

For the radiative cooling rate $\dot{\gamma}_{\rm ave}(\gamma_{\rm ave})$, we use the average radiation power $P_{\rm ave}(\gamma_{\rm ave})$ calculated by equation (40) as

$$\dot{\gamma}_{\rm ave}(\gamma_{\rm ave}) = -\frac{P_{\rm ave}(\gamma_{\rm ave})}{m_e c^2}. \tag{47}$$

The radiation spectrum is calculated as

$$P_\nu(t) = \int_1^\infty d\gamma_{\rm ave}N(\gamma_{\rm ave}, t)P_{\nu,\rm ave}(\gamma_{\rm ave}), \tag{48}$$

where $P_{\nu,\rm ave}(\gamma_{\rm ave})$ is the radiation spectrum calculated with eq. (42).

6.2. *Slow cooling*

The cooling break should appear at $\gamma_{\rm ave} = \gamma_{\rm c}$, which satisfies $t = \gamma_{\rm ave}/\dot{\gamma}_{\rm ave}$. First, we consider the case with $\gamma_{\rm c} \gg \gamma_{\rm cut}$, where the cooling effect is negligible (slow cooling). As we have discussed, the emission properties change at $\gamma_{\rm ave} = \gamma_\lambda$, where γ_λ is the electron Lorentz factor at which the corresponding Larmor radius is comparable to the wavelength,

$$\frac{\gamma_\lambda m_e c^2}{eB_0} = \lambda. \tag{49}$$

As shown in the upper panel of Figure 3, the electron energy distribution for $\gamma_\lambda \ll \gamma_{\rm min}$ (green) is not affected by the wave, and is almost the same as the case without the wave (dashed black). On the contrary, for $\gamma_\lambda \gg \gamma_{\rm cut}$ (blue), all electrons gain energy by the wave, so that the distribution is shifted to higher energies. In the case for $\gamma_{\rm min} < \gamma_\lambda < \gamma_{\rm cut}$ (red), the distribution shows a concave shape connecting the two cases of $\gamma_\lambda \ll \gamma_{\rm min}$ and $\gamma_\lambda \gg \gamma_{\rm cut}$ around $\gamma \simeq \gamma_\lambda = 10^8$.

The lower panel of Figure 3 shows the resultant photon spectra. The spectrum and frequency are normalized by

$$P_{\rm cut} \equiv \frac{4}{3}\gamma_{\rm cut}^2 c\sigma_T \frac{B^2}{8\pi}, \tag{50}$$

and

$$\nu_{\rm cut} \equiv \frac{3}{16}\gamma_{\rm cut}^2 \frac{eB}{m_e c}, \tag{51}$$

respectively. The boost of electron energies for $\gamma_\lambda \gg \gamma_{\rm cut}$ (blue) leads to a slightly higher peak energy in the photon spectrum. However, as the induced electric field suppresses the emissivity (see Figure 2), the energy boost does not enhance the power in the low-frequency regime compared to the case without the wave (dashed black). For $\gamma_\lambda \ll \gamma_{\rm min}$ (green), the emissivity is slightly higher compared to the case without the wave owing to the enhanced acceleration as discussed in §5.

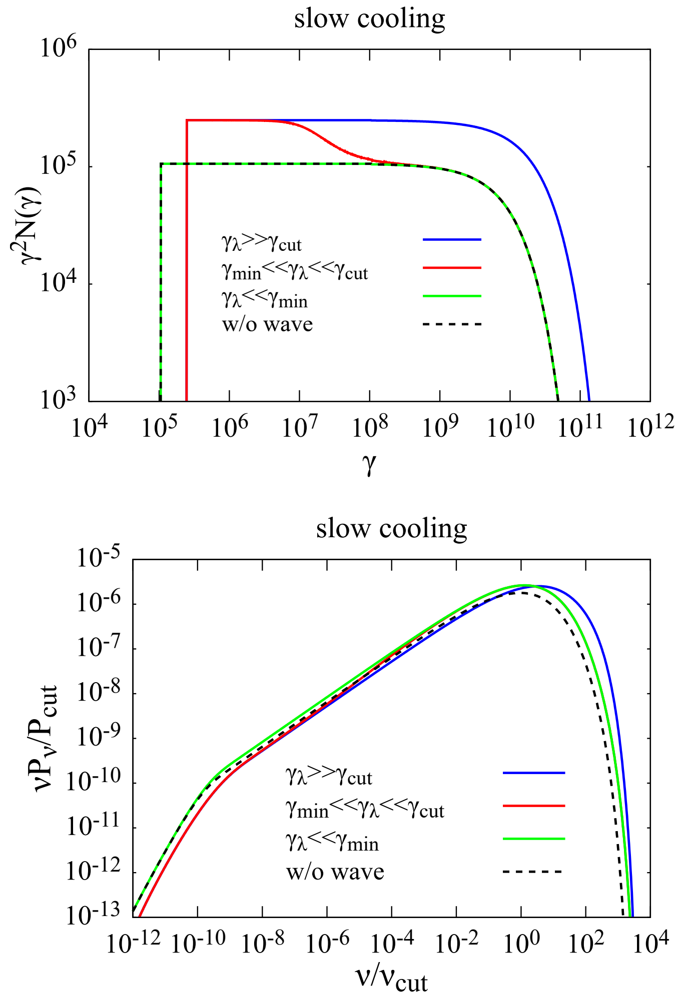

Figure 3. The electron energy distributions (upper) and the radiation spectra (lower) with a power-law ($p = 2$) distribution for injection in the slow cooling case. The colored solid lines show the results for different γ_λ. The case without the wave is shown with the dashed black line.

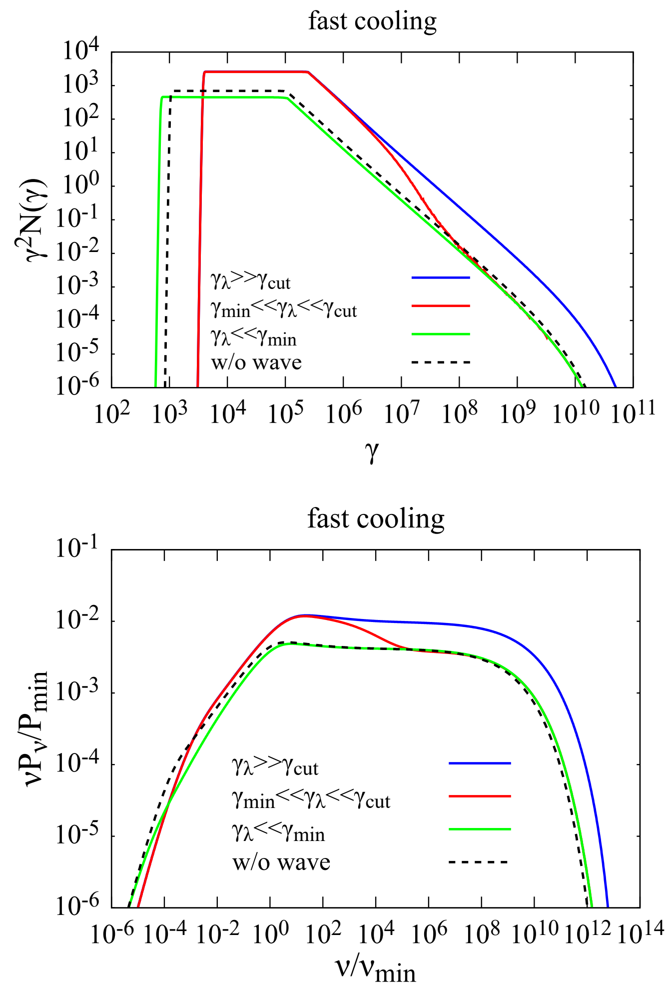

Figure 4. Same as Figure 3 but for the fast cooling case.

For $\gamma_{\rm min} < \gamma_\lambda < \gamma_{\rm cut}$ (red), the radiation spectrum is curved slightly around

$$\nu_\lambda \equiv \frac{3}{16}\gamma_\lambda^2 \frac{eB}{m_e c}, \tag{52}$$

connecting the blue line in low-frequency region and the green line in high-frequency region. However, the modulation is not so prominent.

6.3. *Fast cooling*

For the fast cooling ($\gamma_c \ll \gamma_{\rm min}$) case, the electron energy distribution becomes softer than the injection spectrum, and a low-energy component below $\gamma_{\rm min}$ appears. The upper panel of Figure 4 shows these properties. The low-energy sharp breaks correspond to $\gamma_{\rm min}$. The energy distribution is shifted to higher energies by the induced electric field for $\gamma_\lambda \gg \gamma_{\rm cut}$ (blue). Note that, unlike the slow cooling case, the energy shift for this steeper spectrum leads to a much larger increase of $N(\gamma)$ for a given γ. The low-energy cut-off at $\sim \gamma_c$ is relatively high because of the cooling suppression. The distributions for the other cases (green and red) present similar behaviors to those in the slow-cooling cases, though the differences in the cooling efficiency appear in the different low-energy cut-offs.

The normalization for the lower panel of Figure 4 is similar to the slow cooling case with

$$P_{\rm min} \equiv \frac{4}{3}\gamma_{\rm min}^2 c\sigma_T \frac{B^2}{8\pi}, \tag{53}$$

$$\nu_{\rm min} \equiv \frac{3}{16}\gamma_{\rm min}^2 \frac{eB}{m_{\rm e}c}. \tag{54}$$

The spectral power for $\gamma_\lambda \gg \gamma_{\rm cut}$ is high compared to the case without the wave, even though the radiation power is relatively suppressed by the induced electric field. This is due to the large increase of $N(\gamma)$ by the energy shift for a steep energy distribution as we mentioned. Even in the slow cooling case, this enhancement of emissivity can be expected for a steep injection spectrum with e.g. $p = 3$. In the case of $\gamma_\lambda \ll \gamma_{\rm c}$ shown with the green line, the radiation spectrum is shifted to a slightly higher frequency in the high-frequency region compared to the case without the wave.

In the case of $\gamma_{\rm min} < \gamma_\lambda < \gamma_{\rm cut}$ (red), the spectrum shows a characteristic bump structure due to the distorted electron spectrum. The steeper spectrum above $\sim 10^2\nu_{\rm min}$ extends to two orders of magnitude in ν. The flat component above $\sim 10^6\nu_{\rm min}$ can be misunderstood as an extra synchrotron self-Compton component. In this misinterpretation, spectral modeling would lead to a much lower magnetic field than the actual value.

7. CONCLUSIONS & DISCUSSION

Magnetically dominated outflow has been considered for pulsar winds, blazar jets, and gamma-ray bursts. Relativistic turbulence in highly magnetized plasma should induce electric fields with a large amplitude. While the standard synchrotron emission has been adopted for the model of emission from such objects, the large electric field induced in the outflows can affect the emission process from relativistic electrons.

As the first step to investigate the emission processes in relativistic turbulence, we have considered circularly polarized Alfvén waves in this paper. We have calculated the radiation spectrum by numerically following the electron trajectories in the waves, which can be analytically expressed. We have shown the energy dependence of the emission power and spectrum from a single electron. For electrons whose Larmor radius is significantly smaller than the wavelength of the turbulence $r_{\rm L0} \ll \lambda$, the motional electric field suppresses the emission power by a factor of $1/\Gamma_{E\times B}^4$, where $\Gamma_{E\times B}$ is the Lorentz factor for the $E \times B$ drift motion. The value of $\Gamma_{E\times B}$ can be significantly large in relativistic turbulence. However, in the case of the circularly polarized Alfvén wave, $\Gamma_{E\times B}$ is limited to $\sqrt{2}$. Note also that the average energy of electrons injected in the relativistic wave is boosted for $r_{\rm L0} \ll \lambda$. For $r_{\rm L0} \gg \lambda$, the emission power and spectral peak frequency are slightly increased by the wave.

We have also demonstrated the emission spectra from electrons injected with a power-law energy distribution. In the slow cooling case, though the complicated effects mentioned above are entangled, the resultant photon spectrum is not drastically modified. However, for the fast cooling case, the photon spectrum can be concave around ν_λ, which is the typical photon energy emitted by electrons of $r_{\rm L0} \simeq \lambda$.

The resultant spectrum is similar to GRB photon spectra detected with *Fermi*-LAT (Abdo et al. 2009, 2010; Ackermann et al. 2010, 2011; Zhang et al. 2011; Ackermann et al. 2014; Yassine et al. 2017). The extra component detected in the GeV energy range has been interpreted as an SSC (Corsi et al. 2010a,b; Asano et al. 2011; Pe'er et al. 2012) or hadronic cascade component (Asano et al. 2009, 2011; Asano & Mészáros 2011). If this extra component is due to relativistic waves in highly magnetized plasma, the estimate of the magnetic field and typical electron energy can be largely altered. In our demonstration, the caveat is that electrons are assumed to be isotropic and energetic as $r_{\rm L0} \gg \lambda$ at injection. If a wave comes just after the isotropic injection, our setup for the calculation is justified.

If the turbulence itself is responsible for particle injection/acceleration, the locally isotropic power-law injection may not be justified. As shown in Comisso & Sironi (2019), magnetic reconnection leads to an anisotropic particle injection. In such cases, depending on the induced anisotropy, the emission spectra would be modified (Goto & Asano 2022). In addition, multiple interactions with Alfvén waves lead to reacceleration (e.g. Stawarz & Petrosian 2008; Teraki & Asano 2019), which can also produce hard photon spectra in GRBs (Asano & Terasawa 2009, 2015; Xu & Zhang 2017), blazars (Lefa et al. 2011; Asano et al. 2014; Asano & Hayashida 2018), and pulsar wind nebulae (Tanaka & Asano 2017; Tanaka & Kashiyama 2023). Those combined effects lead to non-trivial shapes of photon spectra.

Though the existence of electrons with $r_{\rm L0} \gg \lambda$ is also non-trivial, there are several setups favorable for generating such high-energy electrons. For example, electrons are accelerated by the electric field due to the vacuum gap in the black hole magnetosphere (e.g. Neronov & Aharonian 2007), then such electrons can be injected into a magnetically driven jet outside. In this case, the injection process and turbulence property in the emission site are independent. Another possible injection mechanism is magnetic reconnection and succeeding re-acceleration. In this case, the injection scale of turbulence λ is comparable to the scale of magnetic islands $l_{\rm MI}$. The induced electric field at the reconnection site is roughly comparable to the background magnetic field. The typical initial energy of accelerated electrons is $E_{\rm typ} \sim eEl_{\rm MI} \sim eB\lambda$. The Larmor radii of electrons accelerated directly with the electric field in magnetic islands can be the same scale as the magnetic islands as $r_{\rm L0} = E_{\rm typ}/(eB) \sim \lambda$ (Bessho & Bhattacharjee 2012; Sironi & Spitkovsky 2014; Comisso & Sironi 2019).

These electrons can be further accelerated via stochastic non-gyro-resonant scattering off the turbulent fluctuations (e.g. see Hoshino 2012; Comisso & Sironi 2019). Such a process may cause an effective injection of electrons with $r_{\rm L0} \gg \lambda$.

While we have focused on circularly polarized Alfvén waves in this paper, our next step will be the investigation of emission in more general turbulence. Especially for relativistic compressible waves, $\Gamma_{E\times B}$ can be significantly large. The induced large electric field may greatly modify the radiation spectrum.

We first appreciate the advice from the anonymous referee. We also thank Kosuke Nishiwaki, Yo Kusafuka, Tomoki Wada, Takumi Ohmura, Tomohisa Kawashima, Tomoya Kinugawa, Kyohei Kawaguchi for useful comments and discussion. R.G. acknowledges the support by the Forefront Physics and Mathematics Program to Drive Transformation (FoPM). This work is supported by the joint research program of the Institute for Cosmic Ray Research (ICRR), the University of Tokyo, and KAKENHI grant Nos. 22K03684, and 23H04899 (K.A.). Numerical computations were in part carried out on FUJITSU Server PRIMERGY CX2550 M5 at ICRR.

APPENDIX

A. RADIATION OF ELECTRONS INJECTED ISOTROPICALLY INTO UNIFORM FIELDS

Electrons are injected isotropically with Lorentz factor $\gamma_{\rm i}$ into a uniform electric field $\boldsymbol{E} = E\boldsymbol{e_y}$ and a magnetic field $\boldsymbol{B} = B\boldsymbol{e_z}$. The components of the normalized velocity $\boldsymbol{\beta} = \frac{\boldsymbol{v}}{c}$ are $\beta_x = \beta_0\cos\theta$, $\beta_y = \beta_0\sin\theta\cos\phi$ and $\beta_z = \beta_0\sin\theta\sin\phi$. The velocity of the $E\times B$ drift motion is $\boldsymbol{v}_{E\times B} = c\frac{\boldsymbol{E}\times\boldsymbol{B}}{B^2} = c\frac{E}{B}\boldsymbol{e_x}$. In the drifting frame, the electron motion is spiral one around the magnetic field $\boldsymbol{B'} = \frac{B}{\Gamma_{E\times B}}\boldsymbol{e_z}$. Hereafter, the prime ' denotes quantities in the drifting frame. The Lorentz factor is given by

$$\gamma(\theta,\phi,t) = \Gamma_{E\times B}\gamma'(1+\beta_{E\times B}\beta'_x), \tag{A1}$$

where $\beta_{E\times B} \equiv \frac{E}{B}$, $\Gamma_{E\times B} \equiv \frac{1}{\sqrt{1-\beta_{E\times B}^2}}$, $\beta'_x = \beta'\sin\alpha'\cos(\omega'_B t')$, α' is the pitch angle between the electron velocity and the magnetic field, and $\omega'_B = \frac{eB'}{\gamma' m_e c}$ is the gyro frequency.

We average $\gamma(\theta,\phi,t)$ over the period of $E\times B$ drift $T_{E\times B} = \Gamma_{E\times B}T'_{\rm gyro}$ where $T'_{\rm gyro} = \frac{2\pi}{\omega'_B}$ is the gyro period. Then,

$$\begin{aligned}\langle\gamma(\theta,\phi)\rangle_t &\equiv \frac{1}{T_{E\times B}}\int_0^{T_{E\times B}}\gamma(\theta,\phi,t)dt = \frac{1}{\Gamma_{E\times B}T'_{\rm gyro}}\int_0^{T'_{\rm gyro}}\Gamma_{E\times B}^2\gamma'(1+\beta_{E\times B}\beta'_x(t'))^2dt' \\ &= \Gamma_{E\times B}\gamma'\left(1+\frac{1}{2}\beta_{E\times B}^2\beta'^2\sin^2\alpha'\right). \end{aligned}\tag{A2}$$

Using $\gamma' = \Gamma_{E\times B}\gamma_{\rm i}(1-\beta_{E\times B}\beta_0\cos\theta)$, $\beta'^2\sin^2\alpha' = \beta_x'^2+\beta_y'^2$ and the Lorentz transformation of velocities $\beta'_x = (\beta_x-\beta_{E\times B})/(1-\beta_{E\times B}\beta_x)$ and $\beta'_y = \beta_y/\Gamma_{E\times B}(1-\beta_{E\times B}\beta_x)$, we obtain

$$\langle\gamma(\theta,\phi)\rangle_t = \Gamma_{E\times B}^2\gamma_{\rm i}f(\theta,\phi), \tag{A3}$$

where

$$f(\theta,\phi) = (1-\beta_{E\times B}\beta_0\cos\theta)\left[1+\frac{1}{2}\beta_{E\times B}^2\left\{\frac{(\beta_0\cos\theta-\beta_{E\times B})^2}{(1-\beta_{E\times B}\beta_0\cos\theta)^2}+\frac{\beta_0^2\sin^2\theta\cos^2\phi}{\Gamma_{E\times B}^2(1-\beta_{E\times B}\beta_0\cos\theta)^2}\right\}\right]. \tag{A4}$$

The angle-averaged Lorentz factor is obtained as

$$\begin{aligned}\gamma_{\rm ave} &\equiv \frac{1}{4\pi}\int_0^{2\pi} d\phi \int_0^{\pi} d\theta \sin\theta \langle \gamma(\theta,\phi)\rangle_t \\ &= \Gamma_{E\times B}^2 \gamma_{\rm i} g(\beta_{E\times B}),\end{aligned} \tag{A5}$$

where

$$g(\beta_{E\times B}) = \frac{3}{4}(1+\beta_{E\times B}^2) + \frac{1-2\beta_{E\times B}^2+\beta_0^2\beta_{E\times B}^2}{8\Gamma_{E\times B}^2\beta_0\beta_{E\times B}} \ln\frac{1+\beta_{E\times B}\beta_0}{1-\beta_{E\times B}\beta_0} \tag{A6}$$

For $\beta_{E\times B} = 1/\sqrt{2}$ and $\beta_0 \simeq 1$, $g(\beta_{E\times B}) \simeq 1.20$. As shown in Figure 5, $\gamma_{\rm ave}$ is boosted from injected Lorentz factor $\gamma_{\rm i}$ by a factor of $\Gamma_{E\times B}^2$ for $\Gamma_{E\times B}\beta_{E\times B} \gg 1$.

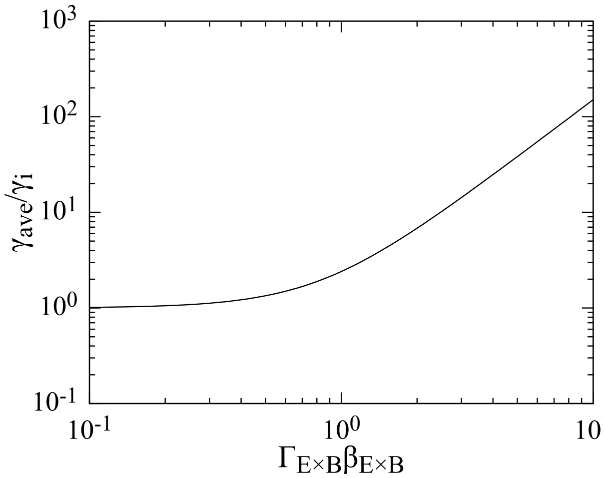

Figure 5. The average Lorentz factor $\gamma_{\rm ave}$ of electrons, which are isotropically injected with $\gamma_{\rm i}$.

Next, we estimate the radiation power. In the drifting frame, the radiation power is constant. As the radiation power is Lorentz invariant, the radiation power in the original frame is also constant and equal to the synchrotron power in the drifting frame. The radiation power of an electron with injection angle θ, ϕ is

$$P(\theta,\phi) = 2c\sigma_T \frac{B'^2}{8\pi}\gamma'^2\beta'^2\sin^2\alpha' = 2c\sigma_T\frac{B^2}{8\pi}\gamma_{\rm i}^2\left\{\left(\beta_0\cos\theta - \beta_{E\times B}\right)^2 + \frac{\beta_0^2\sin^2\theta\cos^2\phi}{\Gamma_{E\times B}^2}\right\}. \tag{A7}$$

The average power is calculated as

$$P_{\rm ave} \equiv \frac{1}{4\pi}\int_0^{2\pi} d\phi\int_0^{\pi} d\theta\sin\theta P(\theta,\phi) = 2c\sigma_T\frac{B^2}{8\pi}\gamma_{\rm i}^2 h(\beta_{E\times B}), \tag{A8}$$

where

$$h(\beta_{E\times B}) = \frac{1}{3}\beta_0^2 + \beta_{E\times B}^2 + \frac{1}{3}\frac{\beta_0^2}{\Gamma_{E\times B}^2}. \tag{A9}$$

Using equations (A5) and (A8), we obtain

$$P_{\rm ave} = 2c\sigma_T\frac{B^2}{8\pi}\gamma_{\rm ave}^2\frac{1}{\Gamma_{E\times B}^4}\frac{h(\beta_{E\times B})}{g(\beta_{E\times B})^2}. \tag{A10}$$

The results are plotted in **Figure 6**, which shows the suppression of the radiative cooling by a factor of $1/\Gamma_{E\times B}^4$ as discussed in the section 2.

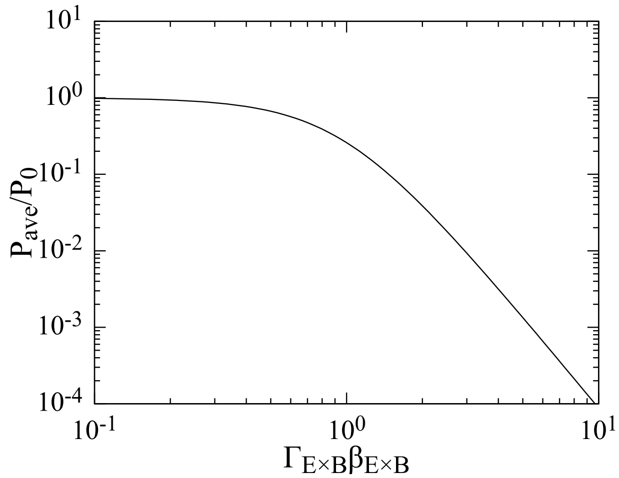

Figure 6. The average radiation power of electrons normalized by P_0.

REFERENCES

Abdo, A. A., Ackermann, M., Ajello, M., et al. 2009, ApJL, 706, L138, doi: 10.1088/0004-637X/706/1/L138

—. 2010, ApJ, 712, 558, doi: 10.1088/0004-637X/712/1/558

Ackermann, M., Asano, K., Atwood, W. B., et al. 2010, ApJ, 716, 1178, doi: 10.1088/0004-637X/716/2/1178

Ackermann, M., Ajello, M., Asano, K., et al. 2011, ApJ, 729, 114, doi: 10.1088/0004-637X/729/2/114

—. 2014, Science, 343, 42, doi: 10.1126/science.1242353

Asano, K., Guiriec, S., & Mészáros, P. 2009, ApJL, 705, L191, doi: 10.1088/0004-637X/705/2/L191

Asano, K., & Hayashida, M. 2018, ApJ, 861, 31, doi: 10.3847/1538-4357/aac82a

Asano, K., & Mészáros, P. 2011, ApJ, 739, 103, doi: 10.1088/0004-637X/739/2/103

Asano, K., Mészáros, P., Murase, K., Inoue, S., & Terasawa, T. 2011, arXiv e-prints, arXiv:1111.0127, doi: 10.48550/arXiv.1111.0127

Asano, K., Takahara, F., Kusunose, M., Toma, K., & Kakuwa, J. 2014, ApJ, 780, 64, doi: 10.1088/0004-637X/780/1/64

Asano, K., & Terasawa, T. 2009, ApJ, 705, 1714, doi: 10.1088/0004-637X/705/2/1714

—. 2015, MNRAS, 454, 2242, doi: 10.1093/mnras/stv2152

Begelman, M. C. 1998, ApJ, 493, 291, doi: 10.1086/305119

Bessho, N., & Bhattacharjee, A. 2012, ApJ, 750, 129, doi: 10.1088/0004-637X/750/2/129

Blandford, R. D., & Znajek, R. L. 1977, MNRAS, 179, 433, doi: 10.1093/mnras/179.3.433

Bromberg, O., & Tchekhovskoy, A. 2016, MNRAS, 456, 1739, doi: 10.1093/mnras/stv2591

Bucciantini, N., Bandiera, R., Olmi, B., & Del Zanna, L. 2017, MNRAS, 470, 4066, doi: 10.1093/mnras/stx993

Comisso, L., & Sironi, L. 2019, ApJ, 886, 122, doi: 10.3847/1538-4357/ab4c33

Comisso, L., Sobacchi, E., & Sironi, L. 2020, ApJL, 895, L40, doi: 10.3847/2041-8213/ab93dc

Corsi, A., Guetta, D., & Piro, L. 2010a, A&A, 524, A92, doi: 10.1051/0004-6361/200912461

—. 2010b, ApJ, 720, 1008, doi: 10.1088/0004-637X/720/2/1008

Fouka, M., & Ouichaoui, S. 2013, Research in Astronomy and Astrophysics, 13, 680, doi: 10.1088/1674-4527/13/6/007

Goldreich, P., & Julian, W. H. 1969, ApJ, 157, 869, doi: 10.1086/150119

Goto, R., & Asano, K. 2022, ApJ, 933, 18, doi: 10.3847/1538-4357/ac67d5

Guo, F., Li, X., Daughton, W., et al. 2019, ApJL, 879, L23, doi: 10.3847/2041-8213/ab2a15

—. 2021, ApJ, 919, 111, doi: 10.3847/1538-4357/ac0918

Guo, F., Liu, Y.-H., Daughton, W., & Li, H. 2015, ApJ, 806, 167, doi: 10.1088/0004-637X/806/2/167

Hakobyan, H., Petropoulou, M., Spitkovsky, A., & Sironi, L. 2021, ApJ, 912, 48, doi: 10.3847/1538-4357/abedac

Hakobyan, H., Philippov, A., & Spitkovsky, A. 2019, ApJ, 877, 53, doi: 10.3847/1538-4357/ab191b

Hoshino, M. 2012, PhRvL, 108, 135003, doi: 10.1103/PhysRevLett.108.135003

Jackson, J. D., & Fox, R. F. 1999, American Journal of Physics, 67, 841, doi: 10.1119/1.19136

Kennel, C. F., & Pellat, R. 1976, Journal of Plasma Physics, 15, 335, doi: 10.1017/S0022377800019863

Lazar, A., Nakar, E., & Piran, T. 2009, ApJL, 695, L10, doi: 10.1088/0004-637X/695/1/L10

Lefa, E., Rieger, F. M., & Aharonian, F. 2011, ApJ, 740, 64, doi: 10.1088/0004-637X/740/2/64

Lyutikov, M. 2010, MNRAS, 405, 1809, doi: 10.1111/j.1365-2966.2010.16553.x

Marscher, A. P. 2014, ApJ, 780, 87, doi: 10.1088/0004-637X/780/1/87

McKinney, J. C., Tchekhovskoy, A., & Blandford, R. D. 2012, MNRAS, 423, 3083, doi: 10.1111/j.1365-2966.2012.21074.x

McKinney, J. C., Tchekhovskoy, A., Sadowski, A., & Narayan, R. 2014, MNRAS, 441, 3177, doi: 10.1093/mnras/stu762

Medvedev, M. V. 2000, ApJ, 540, 704, doi: 10.1086/309374

Mizuno, T., Ohno, H., Watanabe, E., et al. 2023, arXiv e-prints, arXiv:2309.16154, doi: 10.48550/arXiv.2309.16154

Mizuno, Y., Lyubarsky, Y., Nishikawa, K.-I., & Hardee, P. E. 2009, ApJ, 700, 684, doi: 10.1088/0004-637X/700/1/684

—. 2011, ApJ, 728, 90, doi: 10.1088/0004-637X/728/2/90

Nalewajko, K., Uzdensky, D. A., Cerutti, B., Werner, G. R., & Begelman, M. C. 2015, ApJ, 815, 101, doi: 10.1088/0004-637X/815/2/101

Narayan, R., & Kumar, P. 2009, MNRAS, 394, L117, doi: 10.1111/j.1745-3933.2009.00624.x

Neronov, A., & Aharonian, F. A. 2007, ApJ, 671, 85, doi: 10.1086/522199

Pe'er, A., Zhang, B.-B., Ryde, F., et al. 2012, MNRAS, 420, 468, doi: 10.1111/j.1365-2966.2011.20052.x

Petropoulou, M., & Sironi, L. 2018, MNRAS, 481, 5687, doi: 10.1093/mnras/sty2702

Porth, O., & Komissarov, S. S. 2015, MNRAS, 452, 1089, doi: 10.1093/mnras/stv1295

Porth, O., Komissarov, S. S., & Keppens, R. 2014, MNRAS, 438, 278, doi: 10.1093/mnras/stt2176

Reville, B., & Kirk, J. G. 2010, ApJ, 724, 1283, doi: 10.1088/0004-637X/724/2/1283

Rybicki, G. B., & Lightman, A. P. 1979, Radiative processes in astrophysics

Schwinger, J. 1949, Physical Review, 75, 1912, doi: 10.1103/PhysRev.75.1912

Shibata, S., Tomatsuri, H., Shimanuki, M., Saito, K., & Mori, K. 2003, MNRAS, 346, 841, doi: 10.1111/j.1365-2966.2003.07131.x

Shikin, I. S. 1969, Annales de l'I.H.P. Physique théorique, 11, 343. http://eudml.org/doc/75645

Singh, C. B., Mizuno, Y., & de Gouveia Dal Pino, E. M. 2016, ApJ, 824, 48, doi: 10.3847/0004-637X/824/1/48

Sironi, L., & Spitkovsky, A. 2014, ApJL, 783, L21, doi: 10.1088/2041-8205/783/1/L21

Stawarz, Ł., & Petrosian, V. 2008, ApJ, 681, 1725, doi: 10.1086/588813

Takamoto, M., Inoue, T., & Lazarian, A. 2015, ApJ, 815, 16, doi: 10.1088/0004-637X/815/1/16

Tanaka, S. J., & Asano, K. 2017, ApJ, 841, 78, doi: 10.3847/1538-4357/aa6f13

Tanaka, S. J., & Kashiyama, K. 2023, MNRAS, 525, 2750, doi: 10.1093/mnras/stad2504

Tchekhovskoy, A., & Bromberg, O. 2016, MNRAS, 461, L46, doi: 10.1093/mnrasl/slw064

Teraki, Y., & Asano, K. 2019, ApJ, 877, 71, doi: 10.3847/1538-4357/ab1b13

Werner, G. R., & Uzdensky, D. A. 2017, ApJL, 843, L27, doi: 10.3847/2041-8213/aa7892

Wong, K., Zhdankin, V., Uzdensky, D. A., Werner, G. R., & Begelman, M. C. 2020, ApJL, 893, L7, doi: 10.3847/2041-8213/ab8122

Xu, S., & Zhang, B. 2017, ApJL, 846, L28, doi: 10.3847/2041-8213/aa88b1

Yassine, M., Piron, F., Mochkovitch, R., & Daigne, F. 2017, A&A, 606, A93, doi: 10.1051/0004-6361/201630353

Zenitani, S., & Umeda, T. 2018, Physics of Plasmas, 25, 112110, doi: 10.1063/1.5051077

Zhang, B., & Zhang, B. 2014, ApJ, 782, 92, doi: 10.1088/0004-637X/782/2/92

Zhang, B.-B., Zhang, B., Liang, E.-W., et al. 2011, ApJ, 730, 141, doi: 10.1088/0004-637X/730/2/141

Zhdankin, V., Werner, G. R., Uzdensky, D. A., & Begelman, M. C. 2017, PhRvL, 118, 055103, doi: 10.1103/PhysRevLett.118.055103